JOURNAL OF SOLID STATE CHEMISTRY 100, 49–61 (1992)

Site-Selective Fluorescence Spectroscopy of Eu(III) β''-Alumina

A. P. BROWN

Department of Chemistry, Bishop's University, Lennoxville, Quebec, Canada J1M 1Z7

Received November 25, 1991; accepted February 25, 1992

Nonresonantly excited site-selective emission spectra and decay times of 34% exchanged Eu^{3+} β''-alumina are presented. Analysis of the emission spectra, time-resolved spectra, and decay times in terms of the coordination environment in which the Eu^{3+} emitting centers are located indicates that the spectra are due to substitution at mid-oxygen crystallographic sites. Furthermore, resonant excitation of one of the Eu^{3+} centers elucidates an energy level scheme in which the $^7F_1$ level lies approximately 100 cm^{-1} above the $^7F_0$ level. © 1992 Academic Press, Inc.

I. Introduction

In recent years there have been a number of spectroscopic studies of triply ionized rare earth ions in $Na^+\beta''$-alumina of which the main goal has been to investigate the nature of the coordination environment about the rare earth ion. These studies have benefited greatly from the results of X-ray crystallographic studies of fully exchanged samples (*1–3*) which indicate that the rare earth ions occupy two coordination sites in the crystal, namely the 9d and 6c Wyckoff positions of the $R\bar{3}m$ space group. Unfortunately the X-ray results qualify this site occupation as only reflecting an ideal situation and that, in fact, there exists considerable variation in position of not only the rare earth ions but also of the oxygen atoms in the conduction plane.

Given the variation in position it has become commonplace to describe the site occupation as rare earth ions on mid-oxygen (mO) and Beevers–Ross (BR) sites and to implicitly accept that the optical spectra correspond to ions at these positions while allowing for distortion from the ideal structure. The mO and BR positions correspond to substitution at the 9d and 6c sites, respectively. When the exchange conditions produce crystals of less than 100% exchange it is also evident that residual sodium ions in the conduction plane also contribute to the disorder (*4*).

Previous investigations of the absorption spectra of $Nd^{3+}\beta''$-alumina (*5*) and Ce^{3+} β''-alumina (*6*), as well as the excitation and emission spectra of $Eu^{3+}\beta''$-alumina (*7*) and $Ce^{3+}\beta''$-alumina (*6*), have been consistent with the X-ray work since at least two distinct spectra were observed for each ion. In addition, inhomogeneously broadened emission spectra have been observed and are reflective of the disordered site occupation (*8*). These different spectra have been assumed to represent the rare earth ion occupying an mO or BR site and arguments in support of these assignments were ad-

0022-4596/92 $5.00

vanced. At this point the investigators have diverged in their analysis of the spectra; Dunn *et al.* (*5*), Barrie *et al.* (*6*), Saltzberg and Farrington (*7*), and Laberge *et al.* (*9*) have argued that the two different spectra are due to substitution at mO sites and at BR sites, whereas Brown and Simkin have maintained (*10*) that the spectra originate from two distinctly different coordination environments for Eu^{3+} ions on mO sites in addition to substitution at BR sites. However, some caution should be exercised in comparing the spectra of different rare earth ions, since there are differences in the structures of the corresponding β''-aluminas particularly in the percentage site occupations and structural parameters (*1–3*).

This work presents the results of two studies on a crystal of 34% exchanged $Eu^{3+}\beta''$-alumina. In the first study a pulsed dye laser is used to excite different Eu^{3+} centers via the $^5D_2 \leftarrow {}^7F_0$ transition and provides site-selective spectra, time-resolved spectra, and decay times. The second study consists of resonantly exciting the $^5D_0 \leftarrow {}^7F_0$ transition of one site, again employing a pulsed dye laser, to elucidate the assignment of peaks for this site.

II. Experimental

Crystals of 34% exchanged $Eu^{3+}\beta''$-alumina were produced by ion-exchange (*11*) reactions on single crystals of $Na^+\beta''$-alumina. The pure $Na^+\beta''$-alumina crystals were grown by flux evaporation techniques (*12*). The idealized formula of the sample is $Na_{1.20}Eu_{0.16}Mg_{0.67}Al_{10.33}O_{17}$, which corresponds to a doping level of 0.54 mole% Eu^{3+} or 3.9 wt% Eu^{3+}. Prior to the spectroscopic measurements the crystal was rinsed several times with acetone and then several times with methanol. This was followed by a 24-hr drying period in a 200°C oven.

The sample was mounted in an Oxford Instruments CF104 cryostat by gluing it onto a brass plate which also served as a mask. Liquid nitrogen was used so that the sample temperature was maintained at 77 K (±0.1 K typically).

The laser excitation was provided by a longitudinally pumped, tunable, pulsed dye laser based on Littmann's design (*13*). A Coumarin dye solution was used to provide laser output from 456 to 466 nm having linewidths of less than 0.01 nm over this range. The dye laser was pumped by a Lumonics TE-861M-3 excimer laser operating with XeCl.

Fluorescence was analyzed by a ¾-m Spex 1702 monochromator with a 1200 line/mm grating and 100-μm slits providing a bandpass of 0.109 nm over the emission range. The emission signal was detected by a Hamamatsu R928 photomultiplier tube and recorded on an EG&G Princeton Applied Research Model 4400 Signal Processing System. This digital boxcar system allowed emission spectra, time resolved spectra, and fluorescence decays to be recorded. Emission spectra were recorded with a delay of 5 μsec after the laser pulse.

The experimental setup for the resonantly excited spectra consisted of the same apparatus except that a variable delay chopper wheel was inserted between the sample and the emission monochromator. The chopper assembly effectively masked the entrance slit of the monochromator while the laser was fired and then, after a delay of approximately 400 μsec, opened to allow the fluorescence from the sample to be monitored. The emission spectra were recorded 1 msec after the laser pulse. The dye used in the dye laser was a Rhodamine dye which provided a tuning range of 565 to 575 nm with a linewidth of less than 0.01 nm. The monochromator's slits were set at 200 μm, which provided a bandpass of 0.216 nm over the emission range. The spectra are not corrected for the response of either the monochromator nor for the photomultiplier tube.

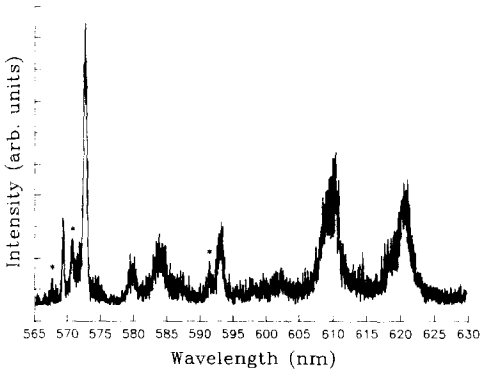

FIG. 1. Emission spectrum of 34% exchanged Eu^{3+} β″-alumina under 457.48-nm excitation at 77 K.

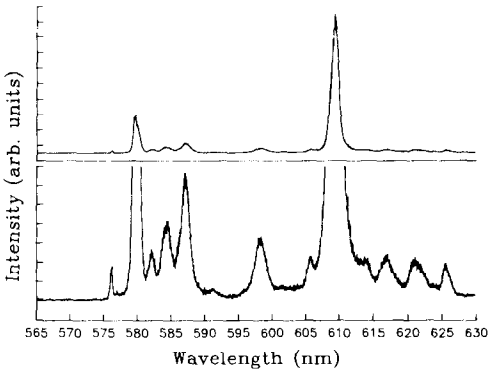

FIG. 3. Emission spectrum of 34% exchanged Eu^{3+} β″-alumina under 463.08-nm excitation at 77 K.

III. Results and Discussion

III.1. Site-Selectivity

The discussion of the experimental results uses a shorthand nomenclature which assigns various features to be due to Eu^{3+} Sites with differentiations expressed as Roman numerals. The reader should be aware that this nomenclature does not refer to distinct crystallographic sites but rather to different Eu^{3+} emitting centers which share similar spectroscopic features. In the present work two types of centers are designated as Site I and Site II.

The results of the site-selective experiments are summarized by the spectra shown in Figs. 1–5. Figures 1 and 2 show the emission spectra produced under 457.48-nm excitation at 77 K, whereas Figs. 3 and 4 show those due to 463.08-nm excitation, also at 77 K. It should be noted that these spectra correspond to maximum emission intensity of the characteristic spectra upon tuning the excitation laser through the $^5D_2 \leftarrow {}^7F_0$ absorption region. Figure 5 shows that spectra characteristic of these two sites are also readily observable at room temperature.

As has been previously demonstrated (*7*, *10*, *14*), these spectra correspond to the types of emitting centers which make up the

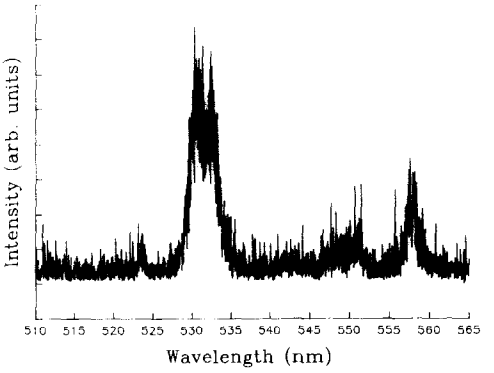

FIG. 2. Emission spectrum of 34% exchanged Eu^{3+} β″-alumina under 457.48-nm excitation at 77 K.

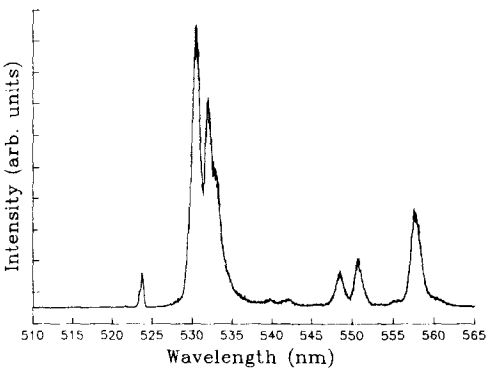

FIG. 4. Emission spectrum of 34% exchanged Eu^{3+} β″-alumina under 463.08-nm excitation at 77 K.

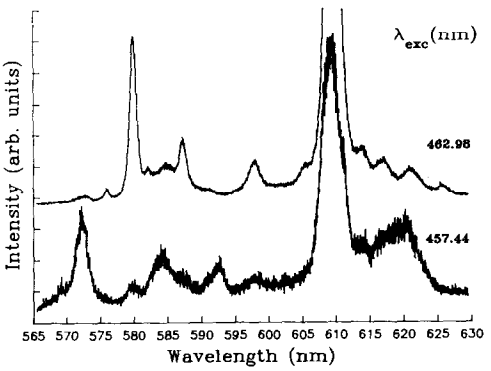

FIG. 5. Emission spectra of 34% exchanged $Eu^{3+}\beta''$-alumina at room temperature.

bulk of the fluorescence due to Eu^{3+} in these materials. It should be noted from the wavelength ranges that some of the emission is originating from higher energy levels than the $^5D_0$ and is presumably originating from the $^5D_1$ and possibly $^5D_2$ levels. This is the first time such emission has been reported in $Eu^{3+}\beta''$-alumina. The interference of such emission can be minimized by identifying it from the decay times or using time-resolved techniques, both of which are discussed later.

The spectra display marked differences in intensity in the $^5D_0 \rightarrow {}^7F_1$ and $^5D_0 \rightarrow {}^7F_2$ regions. Under 457.48-nm excitation the intensity of the $^5D_0 \rightarrow {}^7F_2$ transitions is on the order of that of the $^5D_0 \rightarrow {}^7F_1$ transitions. The centers responsible for spectra of this type are designated Site I. Under 463.08-nm excitation the emission spectrum is dominated by intense $^5D_0 \rightarrow {}^7F_2$ emission as well as very strong $^5D_1 \rightarrow {}^7F_3$ emission, both of which appear to display hypersensitive behavior. These centers are designated to be Site II. Since the Eu^{3+} ion is being used as a structural probe, the reader is reminded of the three general conclusions, reached as the result of extensive studies carried out by Blasse and coworkers (*15–20*), which are relevant in the present context:

(1) The spectral energy distribution is strongly dependent on the site symmetry of the Eu^{3+} ion.

(2) The main emission peaks are due to $^5D_0 \rightarrow {}^7F_1$ and $^5D_0 \rightarrow {}^7F_2$ transitions.

(3) The multiplet splittings were always in agreement with the predicted splittings from the site symmetry.

The reader is reminded that the Eu^{3+}–host combinations were represented by three categories: the presence of strict inversion symmetry, no center of symmetry, and small deviations from inversion symmetry.

The approximately equal distribution of spectral energy in Site I indicates that the Eu^{3+} ion occupies a position having small deviations from inversion symmetry. The substitution site having inversion symmetry in β''-alumina is the mO site (C_{2h}) and therefore this spectrum is assigned as due to mO substitution. This symmetry assignment is consistent with the full splitting, i.e., three components, of the $^5D_0 \rightarrow {}^7F_1$ multiplet. It should be noted that the spectrum of Fig. 1 appears to display "extra" peaks, denoted by asterisks. These are particularly noticeable in the 568- to 575-nm region. This phenomenon, discussed more fully in Section III.4, is due to the energy level scheme of this site which leads to an increased probability of accidental degeneracies when performing experiments at 77 K.

The strong $^5D_0 \rightarrow {}^7F_2$ emission of Site II would appear to indicate that noninversion symmetry exists for these centers. However, this assumption is somewhat clouded by the presence of hypersensitivity, where upon inspection of Fig. 3 it is evident that only one component of the $^5D_0 \rightarrow {}^7F_2$ transition is very intense, the others being visibly on the order of the intensities of the individual components of the $^5D_0 \rightarrow {}^7F_1$ transition. Some indication of the site symmetry can be derived from Judd's analysis (*21*) of hypersensitive transitions in which the phenomenon has been related to the following site symmetries:

C_s, C_1, C_2, C_{2v}, C_3, C_{3v}, C_4, C_{4v}, C_6, C_{6v}.

According to Judd, these site symmetries may allow linear crystal field terms which have been proposed to be a factor in the observation of hypersensitivity as well the intensity of the $^5D_0 \rightarrow {}^7F_0$ forbidden transition. However, since the mechanism, or mechanisms, governing hypersensitivity is not well understood and it remains difficult to come to any absolute conclusions concerning the site symmetry of the emitting center simply based on the appearance of hypersensitivity.

The observation of hypersensitivity alone does not differentiate between C_2 (mO) and C_{3v} (BR) symmetry using Judd's criteria. However, the full splitting of the $^5D_0 \rightarrow {}^7F_1$ and $^5D_0 \rightarrow {}^7F_2$ multiplets, three and five components, respectively, aids in assigning this spectrum to mO sites of C_2 symmetry. It should be noted that this assignment remains consistent with other investigators' assignments (*4*, *7*) but differs from Dai and Stafsudd's conclusions for Nd^{3+} β″-alumina (*22*).

If either of the observed emission spectra were due to BR substitution then the site symmetry would dictate two $^7F_1$ and three $^7F_2$ components. Allowing for disorder in the structure would perhaps lead to more splitting than in the ideal site symmetry, but the splitting pattern would still be dominated by the nearest-neighbor coordination, C_{3v} or perhaps C_3, and this should lead to small energy splittings between components descended from the higher symmetry. Indeed, this procedure, known as descending symmetries, is commonly used when analyzing the spectra of Eu^{3+} ions in crystals and glasses. Small energy splittings in component peaks have been observed for spectra previously assigned to BR substitution in β″-alumina (*10*) and are not apparent in either of the emission spectra presented here.

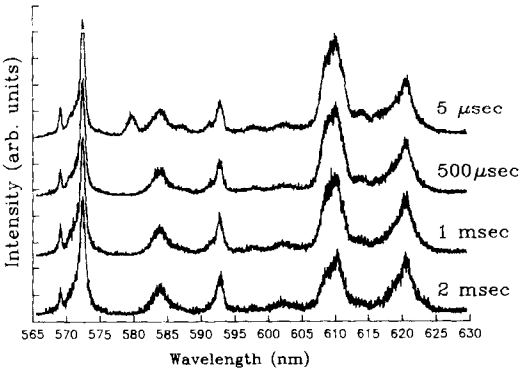

FIG. 6. Time-resolved emission spectrum of 34% exchanged Eu^{3+} β″-alumina under 457.42-nm excitation at 77 K. Time delay after excitation is indicated above each spectrum.

III.2. Time-Resolved Spectra

In an attempt to eliminate interference from the emission from higher energy states than $^5D_0$, the spectra representative of the two emitting centers were time-resolved. These time-resolved spectra are illustrated in Figs. 6 and 7. The notable features of the spectra produced under 457.42-nm excitation are the rapid disappearance of emission originating from $^5D_1$ levels and the steady decrease in intensity of emission in the

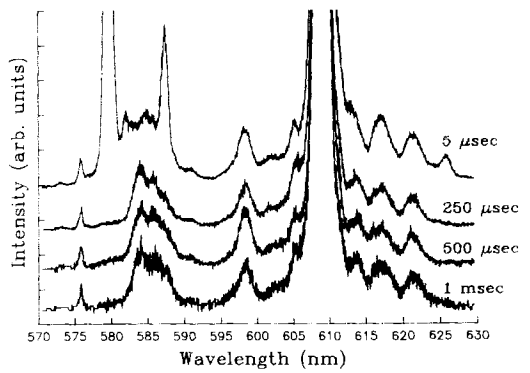

FIG. 7. Time-resolved emission spectrum of 34% exchanged Eu^{3+} β″-alumina under 462.90-nm excitation at 77 K. Time delay after excitation is indicated above each spectrum.

$^5D_0 \rightarrow {}^7F_2$ region relative to the intensity of the $^5D_0 \rightarrow {}^7F_1$ transitions. These two features are in fact due to pseudodiffusion (*23*), which is the result of the very large oscillator strength of the $^5D_2 \leftarrow {}^7F_0$ transition of Site II. This site is the origin of the $^5D_1 \rightarrow {}^7F_J$ emission as well as the hypersensitive $^5D_0 \rightarrow {}^7F_2$ band at approximately 610 nm. Since the emission of this site decays faster than that of Site I, time-dependent behavior of the emission spectrum occurs. While it is obvious that true site-selection is not achieved in this case, at long delay times, the time-resolved spectrum approaches that due solely to Site I.

The time-resolved spectrum produced under 462.90-nm excitation also allows separation of $^5D_1 \rightarrow {}^7F_J$ emission from $^5D_0 \rightarrow {}^7F_J$ emission due to the faster decay time. Otherwise the spectra do not exhibit any variation with increasing delay time.

Certainly the time-resolved spectra presented here are subject to limitations. For instance, since accidental degeneracies are unavoidable due to the $^5D_2 \leftarrow {}^7F_0$ pumping scheme, resonant energy transfer is expected to take place. Unfortunately this would not necessarily be reflected in the spectra. Secondly, if cross-relaxation and energy migration occur on a time scale much less than 5 μsec then the spectra would reflect only the decay of these equilibrium emitting centers.

The greatest asset of the time-resolved spectra presented here is that the spectra at long delay times may be used to analyze the peak positions and spectral intensities with reduced interference. The spectrum recorded at 2 msec delay under 457.42-nm excitation was used to provide the peak assignments and intensities as given in Tables I and II. Table III gives the corresponding values of multiplet intensities for 462.90-nm excitation and 1 msec delay. The peak assignments in most cases were straightforward except for transitions that are seen to be incomplete for Site I, and assignments for Site II were chosen to be consistent with other investigations on the same sample (*24*). Discussion of the spectral intensities is deferred until the next section.

TABLE I
PEAK POSITIONS AND ASSIGNMENTS

	Wavelength (nm) Site I[a]	Site II[b]
$^5D_0 \rightarrow {}^7F_0$	569.88	575.84
$^5D_0 \rightarrow {}^7F_1$	573.24	583.96
	584.68	586.80
	593.59	598.33
$^5D_0 \rightarrow {}^7F_2$	603.31	605.41
	609.41	609.00
	—	613.87
	—	616.93
	621.41	621.53

[a] 457.42-nm excitation.
[b] 462.90-nm excitation.

III.3. Decay Times

The analysis of fluorescence decay times is relevant in the present case since the structural differences which affect the spectral intensity distribution should be reflected in differences in measured decay times. The $^5D_0 \rightarrow {}^7F_J$ decay times will be considered since only one initial state is involved which greatly simplifies the analysis. It is well known that in theory, the radiative lifetime, τ^R, of emission from an initial state a to terminal states b is given by

$$\frac{1}{\tau^R} = \sum_b A_{ab}, \tag{1}$$

where A_{ab} is the spontaneous emission probability for the transition from a to b with the sum extending over all terminal levels b. Since the intensity, I_{ab}, of a radiative transition is related to A_{ab} via

$$I_{ab} = N_a h c \nu A_{ab}, \tag{2}$$

TABLE II

MULTIPLET INTENSITIES FOR SITE I

Transition	Wavelength Range (nm)	Area (arb. units)	ν (cm^{-1})	$A'(s^{-1})$
$^5D_0 \rightarrow {}^7F_0$	568–570	1.34×10^1	17575	0.00590
$^5D_0 \rightarrow {}^7F_1$	570–597	2.21×10^2	17138	1.00
$^5D_0 \rightarrow {}^7F_2$	597–628	2.72×10^2	16327	1.29

where N_a is the population of the initial state, h is Planck's constant, c the speed of light, and ν the frequency of the radiation in cm^{-1}, it becomes evident that the expected fluorescence decay time will depend upon the partitioning of the spectral intensity from the initial level to the terminal levels.

Considering the special case of emission originating from the $^5D_0$ level of Eu^{3+}, the nature of the emission spectrum and decay times may be used to argue for or against the presence of an inversion center in the emitting site. It is well known that magnetic-dipole transitions within the $4f^6$ configuration are fully allowed by Laporte's rule and are subject to the selection rule

$$\Delta J = 0, \pm 1 \text{ (not } 0 \leftrightarrow 0).$$

The pertinent transition is then $^5D_0 \rightarrow {}^7F_1$ and since, to a first approximation, its intensity does not depend upon the site symmetry the intensity of this transition may be used as a standard to measure other transitions against.

Sites having noninversion symmetry allow electric-dipole transitions which in the case under discussion are subject to the selection rules

$$|\Delta J| = 2, 4, 6.$$

It is also well known that noninversion sites show strong electric-dipole emission relative to magnetic-dipole emission. In addition, note that the preceding argument neglects the effect of J-mixing on the spectral intensities.

The emission originating from the $^5D_0$ levels of both sites is normalized to the $^5D_0 \rightarrow {}^7F_1$ intensity, $I_{ab'}$, via

$$\frac{I_{ab}}{I_{ab'}} = \frac{\nu_{ab} A_{ab}}{\nu_{ab'} A_{ab'}}, \tag{3}$$

where ν_{ab} is the frequency of the transition in cm^{-1} and b' refers to the special case when $b = 1$. Giving $A_{ab'}$ and arbitrary value of 1.00 sec^{-1} allows an estimate, using Eq. (3), of the relative magnitudes of the decay times of the two identified sites to be made. These calculations are summarized in Tables II and III for the two sites. Note that the spontaneous emission probability is

TABLE III

MULTIPLET INTENSITIES FOR SITE II

Transition	Wavelength range (nm)	Area (arb. units)	ν (cm^{-1})	A' (s^{-1})
$^5D_0 \rightarrow {}^7F_0$	575–577	2.94×10^{-1}	17361	0.0167
$^5D_0 \rightarrow {}^7F_1$	579–600	1.72×10^1	16964	1.00
$^5D_0 \rightarrow {}^7F_2$	600–629	1.64×10^2	16273	9.96

denoted A' to underline the neglect of $^5D_0 \rightarrow {}^7F_{3,4,5,6}$ emission as well as the normalization to 1.00 sec^{-1}.

As expected, the measured decay curves were nonexponential and fitting to a simple exponential function was not able to extract reproducible decay times from the data. This nonexponential behavior has its origin in several different mechanisms. The first is degradation of the site-selectivity, which can be seen to be particularly evident in the case of Site I. In addition to the large oscillator strength of the transition there is also the effect of untuned broad band emission from the laser which excites centers nonselectively. It is also difficult to account for the amount of overlap of the transitions of the distinct sites which contribute to the inhomogeneous absorption profile. These sites would presumably have different lifetimes so that the emission could be considered to be an envelope of a number of exponential decays of differing lifetime. Energy migration, whose effect in the present case is unknown, will also affect the decay times. Lastly, the reader should note that emission originating from the $^5D_1$ and $^5D_0$ states overlaps in certain spectral regions and this constitutes an interference when attempting to determine decay times.

Since nonexponential lifetime behavior had been previously noted in glasses, Brecher and Riseberg's procedure (*25*) is followed and the function used to fit the measured decay curves is

$$\ln I = \ln I_0 - \alpha t + \beta t^2, \qquad (4)$$

where I is the intensity at time t, in seconds, I_0 is the intensity at $t = 0$, and where the decay time is given by

$$\tau = -(\alpha)^{-1}. \qquad (5)$$

The measured decay times under both excitation wavelengths are given in Tables IV and V. Inspection of the measured decay times show that emission from Site I is longer lived than that from Site II, the decay times for Site I being on the average about 3.40 msec, whereas for Site II they are remarkably constant at about 940 μsec. The variation in measured decay times for Site I is presumably due to several factors: the increased noise level relative to Site II, the inherent variations of different components of multiplets, and the accidental degeneracies which degrade the site-selectivity. Emission originating from $^5D_1$ levels is readily identified by the shorter lifetimes relative to $^5D_0$. The close agreement of the decay times from $^5D_1$ levels for both excitations indicate that the emission is due to Site II and that it can be considered as an interference in the spectra attributed to Site I. In addition, the anomalous value for the 610-nm peak under 457.48-nm excitation is due to interference from strong $^5D_0 \rightarrow {}^7F_2$ emission from Site II. These observations are the result of the strong oscillator strength of the $^5D_2 \leftarrow {}^7F_0$ transition as discussed in Sec. II.

As expected, the site excited under 457.48-nm excitation possesses the longer calculated decay time, on the order of 4.8 times longer than that of the site excited by 463.08-nm excitation. The ratio for the average of the measured decay times is 3.6, which represents quite good agreement considering the neglect of $^5D_0 \rightarrow {}^7F_{3,4,5,6}$ emission, the variation in measured decay

TABLE IV

DECAY TIMES UNDER 457.48-nm EXCITATION

λ_{em}(nm)	τ	Assignment
530.70	26.2 μs	$^5D_1 \rightarrow {}^7F_1$
558.20	29.4 μs	$^5D_1 \rightarrow {}^7F_2$
569.31	3.34 ms	$^5D_0 \rightarrow {}^7F_0$
572.70	4.07 ms	$^5D_0 \rightarrow {}^7F_1$
579.51	29.6 μs	$^5D_1 \rightarrow {}^7F_3$
583.90	3.00 ms	$^5D_0 \rightarrow {}^7F_1$
593.15	5.00 ms	$^5D_0 \rightarrow {}^7F_1$
610.15	1.61 ms	$^5D_0 \rightarrow {}^7F_2$
620.51	3.26 ms	$^5D_0 \rightarrow {}^7F_2$

TABLE V

DECAY TIMES UNDER 463.08-nm EXCITATION

λ_{em}(nm)	τ	Assignment
523.76	30.5 μs	$^5D_1 \rightarrow {}^7F_0$
530.40	30.4 μs	$^5D_1 \rightarrow {}^7F_1$
532.06	30.9 μs	$^5D_1 \rightarrow {}^7F_1$
548.61	31.3 μs	$^5D_1 \rightarrow {}^7F_2$
550.70	32.9 μs	$^5D_1 \rightarrow {}^7F_2$
557.65	28.9 μs	$^5D_1 \rightarrow {}^7F_2$
576.15	916 μs	$^5D_0 \rightarrow {}^7F_0$
579.40	29.9 μs	$^5D_1 \rightarrow {}^7F_3$
582.06	30.0 μs	$^5D_1 \rightarrow {}^7F_3$
584.31	940 μs	$^5D_0 \rightarrow {}^7F_1$
587.06	885 μs	$^5D_0 \rightarrow {}^7F_1$
598.26	954 μs	$^5D_0 \rightarrow {}^7F_1$
609.36	969 μs	$^5D_0 \rightarrow {}^7F_2$
616.90	941 μs	$^5D_0 \rightarrow {}^7F_2$
621.01	958 μs	$^5D_0 \rightarrow {}^7F_2$
625.56	29.0 μs	$^5D_1 \rightarrow {}^7F_4$

times for Site I, and the inherent approximations of the derivation, particularly in the neglect of the effect of polarization on the intensities of peaks in the spectra. The observed decay times may also be taken as evidence against the Site I spectrum being due to BR substitution. Since BR sites lack an inversion center, the decay times for these sites would be expected to be relatively short, presumably on the order of those observed for Site II. In the face of such contradictory evidence as spectral splitting patterns and measured decay times it is difficult to assign either of the emission spectra to BR substitution.

Inspection of Tables II and III reveals interesting information on the relative intensities, given by A', of the forbidden $^5D_0 \rightarrow {}^7F_0$ transitions for the two sites. In the case of Site I the intensity of the $^5D_0 \rightarrow {}^7F_0$ transition relative to $^5D_0 \rightarrow {}^7F_1$ is about 0.6%, however, for Site II it is on the order of 1.7%. This larger intensity is consistent with the strong $^5D_0 \rightarrow {}^7F_2$ intensity for this site which is presumably being admixed, via J-mixing, into the $^5D_0 \rightarrow {}^7F_0$ transition. In terms of the coordination environment of the Eu^{3+} ion, it suggests that the coordination on one side of the ion is different than on the other (*17*). This picture of the coordination environment of this Site is consistent with the model of Nd^{3+} coordination in β''-alumina proposed by Alfrey *et al.* (*4*).

The proposed picture of the Eu^{3+} coordination, i.e., that mO substitution leads to at least two types of local site symmetries with either the presence of an inversion center or without, displays interesting parallels to the case of Eu^{3+} ions in Y_2O_3. It is well known that the structure of Y_2O_3 consists of a central yttrium atom surrounded by six equidistant oxygen atoms located at six corners of a cube. The possible arrangements of the six oxygen atoms among the eight corners of the cube lead to C_2 sites and C_{3i} (or S_6) substitution sites for Eu^{3+} ions in the ratio 3 : 1. It is found experimentally that emission from C_{3i} sites is longer lived, up to five times longer, than emission from C_2 sites (*26*). As with Eu^{3+} β''-alumina this is also consistent with the spectral intensity distribution. Furthermore, the $^5D_0 \leftrightarrow {}^7F_0$ transition of the C_{3i} site occurs at 577.97 nm, whereas that of the C_2 site occurs at 580.89 nm, an almost 3 nm (87 cm^{-1}) shift to shorter wavelength (*27*). Point-charge lattice sum calculations performed on Y_2O_3 assigned valence charges to the Eu ions of +2.56 for C_{3i} and +1.26 to C_2 sites in order to provide satisfactory agreement between phenomenological and point-charge crystal-field parameters (*28*). The lower charge is attributed to greater covalent bonding possible for ions on C_2 sites. Similar calculations performed on idealized β''-alumina structures have been consistent with Y_2O_3 in that the greater the valence charge assigned to Eu ions the greater the value of the calculated B_{20} and B_{22} parameters (*24*), which in the absence of J-mixing define the total splitting of the $^7F_1$ multiplet (*29*). This is quantitatively in agreement with the assignments of the observed spectra in that the total splitting of

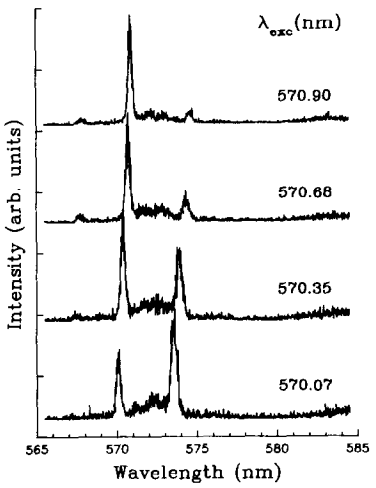

FIG. 8. Examples of resonantly excited spectra of 34% exchanged $Eu^{3+}\beta''$-alumina at 77 K.

the $^7F_1$ multiplet is greater for Site I than for Site II.

III.4. Resonantly Excited Spectra

An effort to test the assignment of the $^5D_0 \rightarrow {}^7F_0$ and $^5D_0 \rightarrow {}^7F_1$ peaks of Site I was conducted by resonantly exciting these transitions by tuning the excitation laser from 567 to 574 nm. A number of the spectra recorded are shown in Fig. 8.

It must be noted that at 77 K the present energy level assignments lead to a population of the $^7F_1$ of 10 to 15% of that of the $^7F_0$ level. In addition, the dipole nature of the transitions differ, $^5D_0 \leftarrow {}^7F_0$ is forbidden, and $^5D_0 \leftarrow {}^7F_1$ is electric-dipole and magnetic-dipole allowed, and hence the intensities of the spectra cannot be attributed solely to population differences.

The most straightforward explanation for the observed spectra is that the excitation, which initially excites the $^5D_0 \leftarrow {}^7F_0$ transition of Site I, is gradually tuned into resonance with the thermally populated $^7F_1$ level of the same site at which point anti-Stokes fluorescence appears. Finally, when the excitation wavelength is long enough it is only in resonance with the $^5D_0 \leftarrow {}^7F_1$ transition of Site I and the Stokes emission disappears.

The proposed energy level scheme is summarized by Fig. 9, in which the resonant, Stokes, and anti-Stokes peaks are plotted relative to a single $^5D_0$ level at 0 cm^{-1}. As can be seen, the resonant peak corresponds to the $^5D_0 \leftrightarrow {}^7F_0$ transition at high excitation frequencies, whereas the Stokes peak corresponds the $^5D_0 \rightarrow {}^7F_1$ transition of the same site. At about 17535 cm^{-1} the appearance of anti-Stokes fluorescence indicates that the excitation has crossed over into the $^5D_0 \leftrightarrow {}^7F_1$ transition with the observed anti-Stokes peaks being the corresponding $^5D_0 \rightarrow {}^7F_0$ transition. Indeed, the energies of the resonant peaks and the anti-Stokes peaks are seen to be equivalent.

Additional evidence that the present peak assignments are correct can be derived from a comparison of the present experiment to one reported by Brown and Simkin in a previous investigation on the same crystal (*10*). In the previous paper a UV laser was employed to nonselectively excite the Eu^{3+} centers, and the resulting spectrum was considered to reflect the inhomogeneously broadened emission from all sites. What is found in the present case is that the energy

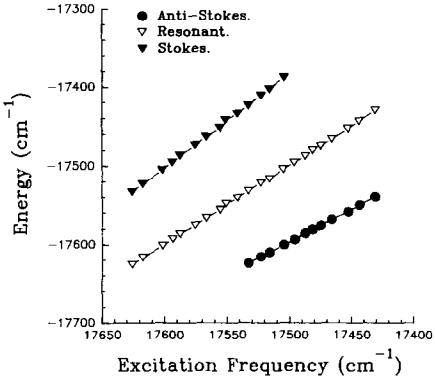

FIG. 9. Plot of resonant line, Stokes, and anti-Stokes emission relative to a $^5D_0$ level at 0 cm^{-1}.

difference between the appearance and disappearance of anti-Stokes emission, corresponding to the range of 567.5 to 570.8 nm, is in very good agreement with the inhomogeneous profile of the peak assigned to $^5D_0 \rightarrow {}^7F_0$ transitions of Site-I-type centers. In addition, the corresponding energy differences for the Stokes emission, which covers the range 570.8 to 575.0 nm, is within the inhomogeneous profile of the $^5D_0 \rightarrow {}^7F_1$ transitions attributed to the same centers.

It is interesting to note that this type of behavior has been observed in glasses in the case of sites having $^7F_1$ components approximately 100 cm^{-1} above the $^7F_0$ level (*25*). The behavior in these cases has also been explained by $^5D_0 \rightarrow {}^7F_0$ anti-Stokes emission accompanying $^5D_0 \leftarrow {}^7F_1$ excitation. In glasses the effect persists at a diminished level even at near helium temperatures so that there is apparently some contribution due to energy transfer. This may also affect the spectra for $Eu^{3+}\beta''$-alumina at lower temperatures.

The similarity in behavior between Eu^{3+}-doped glasses and the present system also extends to the shape of the curves in Fig. 9. Note that the tuning range extends from 17630 cm^{-1} (567.2 nm) to 17430 cm^{-1} (573.7 nm) and that there are no marked dislocations as might be expected if there were large differences in the Eu^{3+} environments. Rather, what is observed is a smooth, continuous change in peak positions which is often associated with amorphous materials. Figure 9 also exhibits a slight divergence of the Stokes and anti-Stokes curves, which indicates a slight change in the crystal-field strength about the ion as the excitation wavelength is varied. This behavior strongly supports a picture of the coordination environment of the Eu^{3+} ions in these sites in β''-alumina as consisting of essentially mO substitution with local variations accounting for the inhomogeneous broadening. As expected, the amount of broadening in the present case is less than is encountered in glasses, since the rigid crystal structure limits the amount of variation in the local crystal-field.

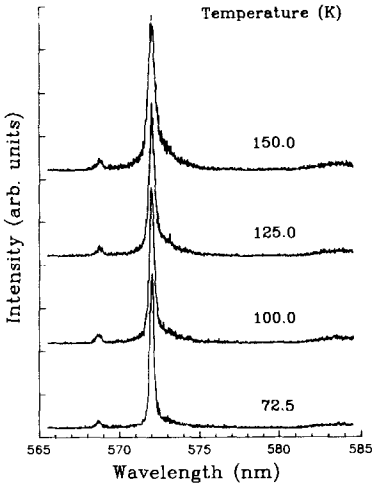

FIG. 10. Temperature dependence of the emission spectrum of 34% exchanged $Eu^{3+}\beta''$-alumina excited at 572.00 nm.

The above assignment of peaks is also found to be appropriate for the temperature dependence of the resonantly excited spectra shown in Fig. 10. The excitation wavelength is 572.0 nm, which primarily excites the $^5D_0 \leftarrow {}^7F_1$ transition of Site I. The intensities of the resonant peak, the anti-Stokes peak, and another peak on the Stokes side of the excitation, identifiable as another $^5D_0 \rightarrow {}^7F_1$ transition, were monitored with increasing temperature. The results show that there is no change in relative intensity of these peaks with increasing temperature, consistent with a thermally populated $^7F_1$ level as the initial level. In addition, the relatively small energy splitting between the $^7F_0$ and $^7F_1$ levels for these sites is responsible for the appearance of extra peaks in Fig. 1, which are due to population of the $^7F_1$ level and subsequent excitement to $^5D_2$ energy levels by the laser. Hence, different crystal-field sites are accidentally probed simultaneously.

IV. Conclusion

The results of the site-selective spectra clearly indicate the presence of two distinctly different Eu^{3+} emitting centers. At present there is no evidence that these two centers account for all the Eu^{3+} substitution sites, or variations within sites, in sodium β''-alumina. The relative intensities of the transitions lead to the conclusion that these centers possess near inversion symmetry (Site I) and noninversion symmetry (Site II). However, these spectra are not simply assigned to mO and BR sites in the crystal, due to the correspondence with the ideal crystal structure, but rather to different types of mO substitution. The main criterion for making these assignments is the full splitting of the multiplets, which contradicts assignment of either Site I or Site II to BR sites of C_{3v} symmetry.

Time-resolved spectra have proved useful in determining the intensities of the emission peaks and also in eliminating interferences due to emission from $^5D_1$ levels and pseudodiffusion. The intensities have also allowed the decay times to be correlated to the spectral energy distribution of the emitting centers and have been shown to be consistent both with the measured decay times and the present assignments of the site symmetries.

The resonantly excited spectra are presented in support of the assignment of peaks for Site I. The energy level scheme suggested by these experiments, i.e., that the lowest component of the $^7F_1$ multiplet lies some 100 cm^{-1} above $^7F_0$, accounts for several anomalous features of the spectroscopy of this Site at 77 K, particularly in the observation of "extra" peaks and the variation in measured lifetimes. It is also noted that in the present assignment there is no need to account for an anomalous intensity of the $^5D_0 \rightarrow {}^7F_0$ transition in the spectra of either Site.

Acknowledgments

The author thanks Professor B. Dunn (UCLA) for kindly providing the 34% exchanged $Eu^{3+}\beta''$-alumina sample. The work presented here was performed at McGill University, Montreal, Quebec, Canada, with facilities provided by Professor D. J. Simkin. Financial assistance from the Natural Sciences and Engineering Research Council of Canada and McGill University is also gratefully acknowledged.

References

1. W. Carillo-Cabrera, J. O. Thomas, and G. C. Farrington, *Solid State Ionics* **9/10,** 245 (1983).
2. B. Dunn, J. O. Thomas, and G. C. Farrington, *in* "Spectroscopy of Solid-State Laser-Type Materials" (B. Di Bartolo, Ed.), pp. 467–474, Plenum, New York (1987).
3. W. Carillo-Cabrera, J. O. Thomas, and G. C. Farrington, *Solid State Ionics* **18/19,** 645 (1986).
4. A. J. Alfrey, O. M. Stafsudd, B. Dunn, and D. L. Yang, *J. Chem. Phys.* **88,** 707 (1988).
5. B. Dunn, D. L. Yang, and D. Vivien, *J. Solid State Chem.* **73,** 235 (1988).
6. J. D. Barrie, L. A. Momoda, B. Dunn, D. Gourier, G. Aka, and D. Vivien, *J. Solid State Chem.* **86,** 94 (1990).
7. M. A. Saltzberg and G. C. Farrington, *J. Solid State Chem.* **83,** 272 (1989).
8. B. Dunn and G. C. Farrington, *Solid State Ionics* **18/19,** 31 (1986).
9. M. Laberge, D. J. Simkin, and B. Dunn, *Chem. Phys. Lett.* **182,** 159 (1991).
10. A. P. Brown and D. J. Simkin, *J. Chem. Phys.* **89,** 5377 (1988).
11. B. Dunn and G. C. Farrington, *Solid State Ionics* **9/10,** 223 (1983).
12. J. L. Briant and G. C. Farrington *J. Solid State Chem.* **33,** 385 (1980).
13. M. G. Littmann, *Opt. Lett.* **3,** 138 (1987).
14. A. P. Brown and D. J. Simkin, *in "Proceedings of SPIE,"* Vol. 929, pp. 44–47, SPIE, Bellingham, WA (1988).
15. W. C. Nieuwpoort and G. Blasse, *Solid State Commun.* **4,** 227 (1966).
16. G. Blasse, A. Bril, and W. C. Nieuwpoort, *J. Phys. Chem. Solids* **27,** 1587 (1966).
17. G. Blasse and A. Bril. *Philips Res. Rep.* **21,** 368 (1966).
18. W. C. Nieuwpoort, G. Blasse, and A. Bril, *in* "Optical Properties of Ions in Crystals" (H. M. Crosswhite and H. W. Moos, Eds.), pp. 161–168, Interscience, New York (1967).

19. G. BLASSE AND A. BRIL, *Philips Tech. Rev.* **31,** 303 (1970).
20. G. BLASSE, *in* "Handbook on the Physics and Chemistry of the Rare Earths" (K. A. Gschneider and L. Eyring, Eds.), Vol. 4, pp. 237–274, North-Holland, Amsterdam (1982).
21. B. R. JUDD, *J. Chem. Phys.* **44,** 839 (1966).
22. H. DAI AND O. M. STAFSUDD, *J. Phys. Chem. Solids* **52,** 367 (1991).
23. P. M. SELTZER *in* "Topics in Applied Physics Vol. 49: Laser Spectroscopy of Solids" (W. M. Yen and P. M. Seltzer, Eds.), pp. 113–140, Springer-Verlag, Berlin, (1986).
24. A. P. BROWN, Ph.D. Thesis, McGill University (1990).
25. C. BRECHER AND L. A. RISEBERG, *Phys. Rev. B* **13,** 81 (1976).
26. H. FOREST AND G. BAN, *J. Electrochem. Soc.* **116,** 474 (1969).
27. J. HEBER, K. H. HELLWEGE, U. KÖBLER, AND H. MURMAN, *Z. Phys.* **237,** 189 (1970).
28. J. B. GRUBER, R. P. LEAVITT, C. A. MORRISON, AND N. C. CHANG, *J. Chem. Phys.* **82,** 5373 (1985).
29. B. PIRIOU, D. FAHMI, J. DEXPERT-GHYS, A. TAITAI, AND J. L. LACOUT, *J. Lumin.* **39,** 97 (1987).